Research Square

Preprints are preliminary reports that have not undergone peer review.
They should not be considered conclusive, used to inform clinical practice,
or referenced by the media as validated information.

Ultra-weak photon emission as a dual-axis probe of dynamized water: physicochemical characterization and germination bioassay

Luis Saluden

luis.saluden@unicaen.fr

Université de Caen Normandie

Olivier Salières

Enerlab

Everyne Van De Kraats

Christophe Carrette

Dynamized Technologies

Article

Keywords:

Posted Date: October 30th, 2026

DOI: https://doi.org/10.21203/rs.3.rs-10766317/v1

License: This work is licensed under a Creative Commons Attribution 4.0 International License.
Read Full License

Additional Declarations: Competing interest reported. C.C. is the founder of Dynamized Technologies, which funded this study. O.S. is affiliated with Enerlab, an independent laboratory commissioned by Dynamized Technologies to conduct the luminometric measurements. L.S. and E.V.d.K. declare no competing interests.

Abstract

Ultra-weak photon emission (UPE) is an established non-invasive probe of aqueous and biological systems, yet technologically dynamized water (TDW) — produced by a vortex–magnetic field processing device (Biodynamizer®) — has not been subjected to systematic luminometric characterization. Using a single photomultiplier tube (PMT) luminometer (Berthold LB9508), we characterized TDW across a physicochemical arm and a germination bioassay — the latter asking whether the physical signal difference translates to a detectable biological response. In the physicochemical arm (N = 47 samples, five water types, four campaigns over six months), TDW emitted 27.5-fold more photons than tap water (n = 11 per group; $p = 8.08\times10^{-5}$; Cliff's $\delta = 1.0$). In the germination bioassay (*Medicago sativa*, 12 germinators, 6 sessions), seedlings irrigated with TDW emitted 4.3-fold more photons than seedlings irrigated with unprocessed tap water at Day 6 (g = 6 germinators per group; $p = 5.1\times10^{-3}$; Cliff's $\delta = 1.0$, days 1–6). Complete stochastic dominance (Cliff's $\delta = 1.0$, meaning every TDW value exceeded every control value) thus held across both a physicochemical and a biological measurement context. The emission mechanism and the coupling pathway from water properties to seed metabolism remain unidentified; this work establishes the observational baseline for mechanistic inquiry.

Introduction

1.1 Ultra-weak photon emission from biological systems

Spontaneous photon emission from biological systems — termed ultra-weak photon emission (UPE) — is detectable in the visible range by photomultiplier tube (PMT) luminometry with typical intensities of tens to several hundred photons per second per square centimetre (photons s^{-1} cm^{-2})[1,2]. Multiple molecular pathways contribute to this emission: triplet-excited carbonyls and singlet oxygen arising from lipid peroxidation[3,4], electron-transfer excited states in the mitochondrial respiratory chain[5], and excited-state intermediates from enzymatic oxidative reactions. The relative contribution of these pathways varies with substrate composition, physiological state, and measurement conditions; UPE is therefore most rigorously treated as a measurement descriptor of photon flux rather than as a direct readout of a single mechanistic pathway[1]. PMT luminometry provides the necessary noise floor for quantitative photon counting and is the instrument standard for this measurement class[2]. Seeds under germination constitute a canonical biological substrate for UPE: cellular respiration resumes upon rehydration, driving the oxidative activity that underlies photon emission, and UPE intensity correlates with germination performance and seed vigour.

Published studies have established UPE as a physiological indicator across the plant kingdom. Spontaneous chemiluminescence from germinating *Arabidopsis thaliana* seeds has been characterized with photon-counting PMT luminometry and shows a distinct temporal profile during imbibition[6]. UPE amplitude in *Helianthus annuus* leaves (N = 206) spans three to four orders of magnitude between control and stress physiological states[7]. Biotic and abiotic stressors in maize induce measurable

changes in spontaneous photon emission[8], and UPE from microorganisms responds systematically to chemical and physical stress agents[9]. For germinating seeds, a reference protocol for time-resolved UPE acquisition has been formalised[10,11]; UPE kinetics track germination performance and seed vigour, and distinguish chemical stress doses within 24 hours of application[12]. Seedling UPE further exhibits chronobiological structure synchronised with the local gravimetric tide[13,14], indicating that UPE reflects a biological state variable beyond acute oxidative load. UPE has further been reported from isolated DNA preparations[15], extending the biological UPE substrate range beyond intact tissue. Both arms of the present study — physicochemical water characterization and germination bioassay — use the same Berthold LB9508 PMT luminometer, providing a common instrumental basis for cross-arm comparison.

1.2 Water-mediated effects on seed UPE and germination

UPE intensity from germinating seeds reflects the quality of the irrigation water[1]. This establishes a precedent for water-property effects on photon emission in a living biological system. Photon-count profiles during wheat germination co-vary with irrigation water quality, including wastewater-derived contaminants[16], and chemically stressed seedlings are distinguishable by UPE kinetics within 24 hours[12,17]. UPE thus functions as a sensitive biological sensor of water-borne physicochemical perturbations; its mechanistic basis remains open.

Beyond irrigation water quality effects traceable to chemical composition, several distinct classes of physically or chemically modified water have been shown to affect seed germination and early plant growth. Plasma-activated water — produced by exposure of water to cold atmospheric plasma discharge — promotes germination rate and seedling vigour in *Erythrina velutina*[18] and lentil (*Lens culinaris*)[19]. Magnetic water treatment, in which water circulates through a static magnetic field before application, improves germination indices and early seedling growth in wheat, barley, and cotton[20–22]. Micro-nano bubble and ultrafine bubble water — characterized by sub-micrometre gas inclusions with extended aqueous persistence — increases crop yield and irrigation water use efficiency under field conditions[23,24] and promotes seed germination directly[25]. Across these modalities, the shared observation is that physical or chemical treatment of water, without altering its gross elemental composition, can produce measurable biological responses in germinating seeds and developing plants.

1.3 UPE as a physicochemical probe of aqueous matrices

The physical basis of UPE — spontaneous emission from electronically excited chemical intermediates — is not specific to biological substrates. PMT luminometry has accordingly been applied to abiotic aqueous matrices[26], establishing measurable signals across oxidative reaction systems, including the sulfite–hydrogen peroxide reaction[27] and the crown ether–Fenton reaction[28]. The emission mechanism is reaction-specific and depends on the chemical substrate. These results establish a methodological precedent for the present study: quantitative UPE luminometry as a physicochemical probe of aqueous matrices.

An epistemic distinction applies between UPE measurements in biological systems and in abiotic aqueous matrices. In biological substrates, chemiluminescence from excited-state reactive oxygen species (ROS) intermediates is the dominant mechanistic framework[1]. This framework provides a useful interpretive context for UPE measurements, though it does not determine the specific molecular contributors, which vary by substrate and physiological state. In abiotic aqueous matrices, the molecular origin of photon emission is more open: no unified mechanistic framework applies, and emission is reaction- and substrate-specific. This study therefore applies UPE strictly as a measurement descriptor — a quantified photon flux — without mechanistic commitment, consistent with the measurement-first approach in the broader UPE literature[1].

1.4 Dynamization: process definition and physicochemical components

Dynamization, as operationally defined in this study, subjects a liquid simultaneously to three physical actions: alternating centripetal vortex rotations (clockwise and counterclockwise), hydrodynamic acceleration-deceleration cycles, and static magnetic field exposure.

Each physical component of dynamization has independent literature support. Static magnetic field exposure modifies surface tension (2–18%), $CaCO_3$ crystallisation polymorph, viscosity, and H-bond geometry, with changes persisting up to two days post-exposure[29–34]. Vortical flow through constrictors generates physicochemical effects via hydrodynamic cavitation: hydroxyl radicals (ROS), mechanical microjets, and local temperatures near 5000 K at bubble collapse[35,36], and enhanced dissolved oxygen concentration through constrained vortex aeration[37–39]. In turbulent flow under simultaneous magnetic field exposure, $CaCO_3$ crystal morphology is further modulated relative to either condition alone[40]. Neither the combined dynamization process nor its individual components has been characterized by ultra-weak photon emission luminometry.

This study follows a geomimetic approach — the designed reproduction of natural abiotic geological processes in a controlled device[41] — by reproducing technologically the hydrodynamic conditions of a geological turbulent transit.

The Biodynamizer® is the technological implementation of this approach. Tap water processed by the Biodynamizer® is referred to hereafter as technologically dynamized water (TDW). The cascade de Vescagne (696 m, Alpes-Maritimes, France) provides the natural geological reference. Water from the Vescagne waterfall is referred to as geologically dynamized water (GDW). Both TDW and GDW fall under the parent category dynamized water. Tap water serves as primary control (TW).

1.5 Hypotheses and scope

Against this background, the present study pursued three complementary objectives. First, we characterized the UPE signature of TDW relative to control waters (TW, mineral bottled water [MBW], and osmosed water [OW]). Second, we examined whether TDW and GDW follow convergent UPE decay

kinetics. Third, we tested whether the UPE elevation observed in the physicochemical arm propagates to a biological response: *Medicago sativa* seeds watered with TDW were compared with seeds watered with TW across multiple germination sessions.

This study characterizes signal differences and tests their statistical distinguishability from control. The mechanism of photon emission in water matrices and the coupling pathway from water properties to seed metabolic activity remain to be identified; candidate hypotheses are addressed as exploratory considerations in the Discussion.

Results

2.1 Physicochemical arm – Comparison of net photon flux density between TDW and TW groups

Technologically dynamized water (TDW), measured immediately after treatment (t_0, no relaxation delay), emitted significantly more photons than tap water (TW) ($p = 8.08 \times 10^{-5}$; $n = 11$ per group; Fig. 1). Cliff's δ = 1.0, a non-parametric effect size (range 0–1), indicates that every TDW value exceeded every TW value. The net photon flux density — photon emission after normalization and subtraction of the instrument background, expressed in relative light units per second per cm² (RLU s^{-1} cm^{-2}) — had a median of 440 RLU s^{-1} cm^{-2} (interquartile range [419; 456], range [369; 603]) for TDW versus 16 RLU s^{-1} cm^{-2} (IQR [12; 22], range [6; 43]) for TW, a 27.5-fold difference (95% confidence interval : 17.0–36.9). Signal-to-noise ratios (SNR) for individual TDW samples ranged from 66 to 108 (median ≈ 79), each exceeding the detection threshold by at least 13-fold (Supplementary Table S1). Cross-campaign reproducibility of TDW emission was confirmed by five consecutive preparations measured in April 2026 (coefficient of variation, CV ≈ 3%).

Over the full dataset of N = 47 samples from four independent measurement campaigns (November 2025 – April 2026), the single fresh GDW (geologically dynamized water; Vescagne waterfall; SNR ≈ 48, Supplementary Table S1) fell within the dynamized range and above all three control water types (Fig. 2). The single-sample status of the GDW measurement, combined with the uncontrolled transit time from collection to measurement (≈ 90–120 min), precludes any inferential or ordinal comparison between TDW and GDW. The dataset supports only the binary distinction between dynamized water (TDW + GDW) and control water (TW, MBW, OW).

Within the control waters, mineral bottled water (MBW; 385 ppm total dissolved solids, TDS) and osmosed water (35 ppm TDS) presented an 11-fold conductivity difference yet differed in net photon flux density by less than 4% (44.75 vs 46.29 RLU s^{-1} cm^{-2}). Dissolved ion concentration is therefore not a determinant of baseline photon emission at the levels present in these samples, and cannot account for the 27.5-fold TDW elevation. This is consistent with the identical source-water TDS of TDW and TW (both drawn from the Nice municipal supply, § 4.2).

2.2 Physicochemical arm – Net photon flux density relaxation kinetics

Net photon flux density in TDW decreased from t_0 toward the tap water baseline over a period of several days (Fig. 3). Linear regression over the active decay phase revealed an approximately linear decline: two independent TDW series measured in February 2026 yielded slopes of − 4.14 and − 4.06 RLU s^{-1} cm^{-2} h^{-1} (R^2 = 0.98 and 0.96 respectively), differing by less than 2%. One GDW series yielded a decay slope of − 3.47 RLU s^{-1} cm^{-2} h^{-1} (R^2 = 0.95), within 16% of the TDW series range. By the 96 h measurement point, all three series had reached the TW global baseline (median 16 RLU s^{-1} cm^{-2}, standard deviation = 10; Fig. 3), consistent with linear fit projections of convergence between 95 h and 103 h. These kinetic results are preliminary (*m*_TDW = 2 series, *m*_GDW = 1 series). The sample size precludes formal comparison of decay rates between water types.

2.3 Germination arm — baseline parity and primary comparison

At D0 (pre-germination baseline, dry seeds before irrigation water was assigned), both groups produced an identical net photon flux density: median 222 RLU s^{-1} cm^{-2} with low inter-group variance (CV < 1%). Pre-treatment equivalence between TDW-assigned and TW-assigned germinators was confirmed. Subsequent measurement sessions differed only in the irrigation water applied.

At the primary endpoint D6, seeds watered with technologically dynamized water (TDW) emitted significantly more photons than seeds watered with tap water (TW) ($p = 5.1 \times 10^{-3}$, Cliff's δ = 1.0; g = 6 germinators per group, where g denotes the number of independent germination chambers; Fig. 4). The TDW group median was 9,107 RLU s^{-1} cm^{-2} versus 2,140 RLU s^{-1} cm^{-2} for TW (ratio 4.3, 95% Confidence Interval [4.1; 4.4]). δ = 1.0 indicates that every TDW-irrigated germinator exceeded every TW-irrigated germinator at D6.

2.4 Germination arm — temporal kinetics D1–D6

The net photon flux density difference between TDW-watered and TW-watered germinators was detectable from the first measurement session (D1) and persisted throughout the germination period (Table 1; Fig. 5). Cliff's δ = 1.0 at every session from D1 to D6. Median net photon flux density in the TDW group increased monotonically from 690 RLU s^{-1} cm^{-2} at D1 to 9,107 RLU s^{-1} cm^{-2} at D6. The TW group remained within a lower band (256–2,140 RLU s^{-1} cm^{-2}) with no systematic monotone trend. The inter-group ratio fluctuated across sessions (2.7-fold at D1, 7.5-fold at D2, 4.3-fold at D6). Complete stochastic dominance was maintained at every time point (Table 1).

Table 1

Longitudinal evolution of UPE in the germination bioassay (June 2026). Per-session group medians (background-subtracted RLU s^{-1} cm^{-2}), TDW/TW median ratio, BCa 95% CI on the ratio (10,000 resamples), Mann-Whitney U, two-sided p, and Cliff's δ. *g* = 6 TDW vs *g* = 6 TW at each session. D = acquisition day.

Session	Median TDW	Median TW	Ratio	BCa 95% CI	U	p	δ
D1	690	256	2.7	[2.5; 2.8]	36	0.0050	1.0
D2	2,655	356	7.5	[7.3; 7.9]	36	0.0050	1.0
D3	2,868	857	3.3	[3.3; 3.4]	36	0.0050	1.0
D4	5,748	858	6.7	[6.6; 6.8]	36	0.0051	1.0
D5	7,806	2,076	3.8	[3.7; 3.8]	36	0.0051	1.0
D6	9,107	2,140	4.3	[4.1; 4.4]	36	0.0051	1.0

2.5 Cross-axis convergence

Both arms yielded complete stochastic dominance — every technologically dynamized water (TDW) value exceeding every tap water value — in the same direction (Cliff's δ = 1.0 in both arms). Water arm: $n = 11$ vs $n = 11$, Mann-Whitney U = 121, $p = 8.08 \times 10^{-5}$. Germination arm: Cliff's δ = 1.0 at every session D1–D6 ($g = 6$ per group). Primary endpoint D6: U = 36, $p = 5.1 \times 10^{-3}$. The two arms differ in substrate (abiotic aqueous matrix vs germinating seedlings) and measurement timescale (single-session vs longitudinal), and share no biological material. The interpretation of this cross-arm pattern is addressed in the Discussion.

Discussion

3.1 Cross-axis convergence and positioning in the UPE literature

The two arms of this study target distinct levels of description with the same instrument. The water arm characterizes the net photon flux density of the abiotic aqueous matrix itself; the germination arm characterizes a biological response of seeds irrigated with that matrix. Both arms returned complete stochastic dominance in the same direction (§ 2.5). The two arms are operationally independent: the water samples and the germinated seedlings were neither prepared, watered, nor measured on the same days, or against the same instrumental baselines. This convergence on two independent modalities is not attributable to a shared methodological source; it constitutes a coherence between a reproducible physical characterization of the intervention and a reproducible biological response to it.

The water arm establishes that the abiotic aqueous matrix exhibits a stable net photon flux density (SNR 66–108) under controlled acquisition. The germination arm establishes that seeds irrigated with that matrix exhibit consistently higher photon emission throughout germination than seeds irrigated with the

same source water prior to processing, at each of the six measurement sessions. The two arms report joint behavior under the same directional effect; the molecular species, electronic transitions, and physiological route that would link them remain to be identified.

This work positions itself relative to three existing strands of the UPE literature. First, the seed UPE / irrigation-water-quality coupling established in § 1.2[1] had not, to our knowledge, been accompanied by an inferential test at adequate sample size on a process-defined dynamized water. The present study supplies that test in both directions: a physicochemical characterization of the water (n = 11 per group) and a biological characterization of the seedlings irrigated with it (g = 6 germinators per group, across six sessions). Second, UPE measured on *Helianthus annuus* seedlings (N = 206) by PMT-based luminometry[7] establishes the biological precedent for the germination arm and the dynamic range expected for green tissues under identical acquisition conditions. Third, PMT-based luminometry applied to abiotic samples ($N = 5$, $p < 0.0001$)[26] establishes the methodological precedent for applying inferential statistics to PMT counts from non-biological aqueous matrices. Together, these three strands confirm that each element of the study design is individually precedented in the UPE literature; the present study is the first to combine all three.

The observation that irrigation water subjected to a physical process — without alteration of gross elemental composition — promotes germination and early plant metabolism is not unique to dynamized water. Plasma-activated water has been shown to increase germination rate and seedling vigour in *Erythrina velutina*[18] and lentil[19]; magnetically treated water improves germination indices in wheat, barley, and cotton[20,21]; ultrafine bubble water promotes germination in direct application[25]. The present germination result is therefore consistent with a pattern observed across mechanistically distinct water modification modalities. What distinguishes this study is the choice of endpoint (photon emission rather than germination rate, shoot length, or dry mass), the dual-arm design that pairs physical characterization of the water with the biological response of the seeds, and the use of a process-defined water in a confirmatory inferential test at adequate sample size. The physical processes underlying plasma activation (reactive oxygen and nitrogen species, UV photons), static magnetic field treatment (hydrogen-bond geometry, $CaCO_3$ polymorph distribution), and turbulent dynamization are sufficiently distinct that convergence at the biological outcome level does not imply equivalence of mechanism; each modality constitutes a separate object of study.

Independent physicochemical characterization of TDW and TW performed by CEBEDEAU on a separately installed device (Supplementary Table S3) confirms that ionic composition cannot account for the observed net photon flux density differential: conductivity, dissolved calcium, magnesium, and total hardness were within 2–5% between groups, and metal leaching (Ag, Cu, Zn) from the device was well below regulatory limits. On-site dissolved O_2 kinetic monitoring (72 h) showed both waters following identical desorption trajectories, with inter-curve differences within sensor precision throughout; the absence of a sustained O_2 differential, combined with the 27.5-fold net photon flux density increase in TDW, argues against a simple dissolved-O_2-mediated emission mechanism. The same analyses

document an enhanced $CaCO_3$ precipitation capacity in TDW (marble test, ASTM standard 2330C; ~16 mg $CaCO_3$ equiv/L), consistent with altered carbonate equilibrium under combined magnetic and hydrodynamic treatment — an observation developed in the geomimetic framing of § 3.2.

3.2 Geomimetic framing and exploratory mechanistic context

The observed decay kinetics is consistent with a non-equilibrium relaxation: the dynamized state, prepared out of equilibrium by turbulent processing, returns toward the equilibrium of the source water, with photon emission as one dissipative channel among others (thermal, acoustic) detectable by luminometry above the visible-range background.

Both TDW (Biodynamizer® output) and GDW (Vescagne waterfall) satisfy the operational definition of dynamization introduced in § 1.3, which justifies a geomimetic framing[41]: the technological process reproduces a property demonstrably produced by its geological counterpart.

The kinetic convergence between TDW and GDW provides empirical support for this framing. TDW exceeds all control waters with complete stochastic dominance (§ 2.1); the single GDW sample falls within the dynamized range. The single-sample status of GDW precludes any TDW–GDW ordinal comparison; the demonstration that dynamized waters exceed controls is the only inferential claim the design supports. The geomimetic argument rests on kinetic similarity, not on amplitude ranking between TDW and GDW: their decay slopes fall within 16% of each other during the active relaxation phase ($R^2 \geq 0.95$, three independent TDW series), a convergence consistent with a shared relaxation trajectory for two processes satisfying the same operational definition (§ 1.3).

The geomimetic framing applies at the conceptual and design level, not in terms of mechanistic equivalence with established geomimetic syntheses[41,42], which operate in hydrothermal regime (100–374°C under pressure) through pathways physically distinct from the ambient-temperature turbulent-flow and magnetic-field processing applied here. Applying this framework to the physical characterization of a water treatment device extends it beyond its established materials-synthesis domain[41,43], a conceptual contribution distinct from the experimental results.

3.3 Limitations and perspectives

Vortex and magnetic field contributions. The Biodynamizer® applies, by construction, simultaneous turbulent flow and static magnetic field; both components produce documented physicochemical effects on water (§ 1.3), and the present design cannot attribute the net photon flux density elevation to either in isolation. A factorial approach — comparing net photon flux density of water treated by turbulent flow alone (magnets removed), static field alone (laminar flow), and the complete cycle — would partition the two contributions and, through systematic variation of flow rate, test whether a monotone process-signal relationship exists, as expected under the geomimetic framing of § 3.2.

Replication scope. All measurements rely on one Biodynamizer® unit, one Berthold LB9508 luminometer, and one laboratory (Enerlab). The kinetic convergence between TDW and GDW argues against an instrumental artefact — a device-specific signal would not selectively converge two dynamized water types — but independent replication remains required. A parallel PMT / charge-coupled device (CCD) acquisition on shared preparations would confirm the net photon flux density measurement across detector types; replication across several Biodynamizer® units would dissociate the process effect from device-specific contributions.

Emission mechanism. The study reports a reproducible photon emission difference and a decay trajectory; the molecular species responsible, the electronic transitions involved, and the dissipation pathway remain uncharacterized. Throughout this article, UPE denotes the luminometric technique and signal magnitude — a measurement descriptor rather than a mechanistic claim, consistent with § 1.4[1]. Hourly sampling over the first 24–48 hours of the active relaxation phase would discriminate between mono- and multi-exponential decay regimes, a distinction the current four-to-five-point series cannot resolve and that would directly constrain candidate mechanistic hypotheses.

Microbial contribution. Tap water contains viable microorganisms that are themselves UPE sources; dynamization might in principle modulate their metabolic activity. Osmosed water — effectively sterile — emitted in the same low-level range as other control waters, which weakens but does not eliminate this hypothesis: OW was represented by a single measurement, precluding statistical comparison. Applying the dynamization protocol to osmosed and distilled water and comparing the resulting net photon flux density against untreated equivalents would provide a direct test of whether the photonic elevation requires a living microbial component.

Germination arm scope. The bioassay tested *Medicago sativa* (alfalfa, organic-certified, ISTA 2021-compliant) across six sessions (g = 6 per group) against a single comparator (tap water); generalisation to other species or control waters is not established. Replication on additional species (e.g. *Triticum aestivum*, *Helianthus annuus*[7]) and against mineral and osmosed water would determine whether the effect extends across botanical families and water types. Non-destructive continuous imaging would simultaneously address the destructive-sampling constraint, enabling within-individual longitudinal tracking unavailable with the current protocol[10].

Morphological observations. Supplementary Figs. S1–S3 document visible differences in aerial growth density, stem height, and root development between groups at D3 and D6; these observations were not quantified and are presented as supplementary documentation only. Image analysis of standardized germinator photographs would convert this qualitative signal into a measurable growth differential and provide a morphological correlate of the net photon flux density difference.

Conclusion

This study provides, to our knowledge, the first dual-arm UPE characterization — physicochemical and biological — of a process-defined dynamized water at inferential sample sizes. Both arms yielded complete stochastic dominance (Cliff δ = 1.0) in the same direction: the physicochemical arm established a stable photonic signature in the abiotic aqueous matrix itself (§ 2.1), and the germination arm established that seeds irrigated with that matrix maintained consistently higher photon emission throughout the full active germination period (§ 2.3–2.4). The coherence of this convergence — across distinct levels of description, distinct sample populations, and distinct acquisition sessions — is the central result and the primary descriptive contribution of the study.

This result fills a gap at the intersection of two literature strands not previously combined on a process-defined dynamized water: the seed UPE / irrigation-water-quality coupling[1] and PMT-based luminometry applied to abiotic aqueous matrices[26]. A second contribution is conceptual: applying the geomimetic design principle — established in materials synthesis — to characterize a water treatment device constitutes, to our knowledge, the first extension of this principle to the technological water treatment context.

The study is at the descriptive phase; the emission mechanism in water and the coupling pathway to seed metabolism remain to be identified. The most direct experimental next step is the factorial decomposition of the turbulent-flow and static-magnetic-field components of the dynamization process — achievable in a modified configuration of the same device — which would move the characterization from process-level observation toward mechanism-level identification.

Methods

4.1 Instrument and acquisition parameters

All photon emission measurements in both study arms were performed on a Berthold LUMAT LB9508 single-tube luminometer (Berthold Technologies, Bad Wildbad, Germany). Samples were measured in borosilicate glass test tubes (3.5 mL volume per sample) in a dark chamber at 20°C. The single-tube dark-chamber geometry, photomultiplier tube (PMT) positioning, and sample-holder configuration relevant to the RLU s^{-1} cm^{-2} normalisation are detailed in Supplementary Methods and illustrated in Supplementary Fig. S4. The instrument firmware normalises raw photon pulse counts by acquisition time and detector area; output is expressed in RLU s^{-1} cm^{-2} (relative light unit, RLU, per second per cm^2), corresponding to photon flux density. This normalisation enables direct within-instrument comparisons across sessions. Acquisition was controlled by the ICE software (Integrated Control and Evaluation, Berthold Technologies). Acquisition parameters were maintained constant across all measurement campaigns; full parameter specifications are proprietary (Enerlab, Nice, France) and are available from the corresponding author upon reasonable request. Eleven consecutive acquisitions (k = 11) were recorded per sample, with an integration time of 10.5 s per acquisition (total sequence duration: 105 s); their arithmetic mean was taken as the representative RLU s^{-1} cm^{-2} value for that sample.

Measurements were conducted in a dedicated laboratory room equipped with an exterior-facing window admitting indirect natural light; the dark-chamber design of the LB9508 isolates the sample from ambient illumination during acquisition. Mobile phones, wirelessly connected devices, and radio-emitting equipment were systematically excluded from the measurement area, and no sources of intentional electromagnetic fields were present near the instrument during any acquisition session. Room layout and equipment placement were held constant across all measurement campaigns to maximise inter-session reproducibility.

4.2 Water arm: sample types and collection

Five water types were characterized: technologically dynamized water (TDW), geologically dynamized water (GDW), tap water (TW), mineral bottled water (MBW), and osmosed water (OW). TDW was produced by the Biodynamizer® device (Dynamized Technologies SA, Braine-le-Château, Belgium); GDW was collected at the Vescagne waterfall (696 m, Alpes-Maritimes, France). TDW and TW both originate from the Nice municipal supply (identical dissolved-solid source), so any UPE difference between these two groups cannot be attributed to differences in source water composition. Independent chemical characterization of TDW and TW confirmed ionic equivalence and the absence of metal leaching from the device (Supplementary Table S3).

All samples were measured within 30 min of collection, except GDW which required a field transit of approximately 90–120 min from the waterfall; GDW samples were collected and transported in translucent glass bottles. Light exposure and handling conditions were kept symmetric across all water types measured at the laboratory (TDW, TW, MBW, OW). For measurement campaigns spanning multiple days or months, samples were stored between acquisition sessions in the same hermetically sealed translucent glass flasks, maintained at constant room temperature and protected from light in a closed metal cabinet between sessions.

A total of $N = 47$ water samples were collected and measured across four independent measurement campaigns: November 2025, December 2025, February 2026, and April 2026. The dataset analyzed here integrates all four measurement campaigns, with the primary statistical comparison involving n = 11 independent TDW (t_0) samples versus n = 11 independent TW samples. Per-session background was determined from empty test tube measurements conducted in the same session. Per-sample raw acquisition values (11 replicates per sample) and campaign metadata for the full $N = 47$ dataset are provided in Supplementary Table S1.

4.3 Water arm: relaxation kinetics series

To characterize UPE temporal decay in TDW and GDW, serial measurements were performed with acquisition at multiple time points following preparation or collection. Four independent series were conducted: two TDW preparation series, one GDW series, and one TW series, each measured once every 24 h over a 7-day period. Between measurement sessions, samples were stored in hermetically sealed translucent glass flasks at constant room temperature and protected from light in a closed metal cabinet, consistent with the inter-session storage conditions described in § 4.2.

Decay curves were modelled by ordinary least squares (OLS) linear regression applied to background-subtracted net RLU s^{-1} cm^{-2} values as a function of elapsed time (hours). The regression yielded slope (RLU s^{-1} cm^{-2} h^{-1}), intercept, and coefficient of determination R^2. OLS was preferred over exponential or piecewise models given the small number of time points per series, which preclude stable estimation of additional parameters.

4.4 Germination arm: seed material and watering protocol

Alfalfa seeds (*Medicago sativa* L.) were germinated in 12 identical germination chambers: six watered with TDW and six watered with TW. Seeds were sourced from a single commercial batch; each germinator received 10 g of seeds (~ 5000 seeds at a thousand-seed mass of approximately 2 g) prior to the campaign start. At each measurement session, 24 seeds or sprouts were extracted from the designated germinator and transferred to the acquisition tube (see § 4.5). All 12 germinators were maintained under identical light, temperature (20 ± 2°C, conforming to the ISTA 2021 protocol for *Medicago sativa* (International Seed Testing Association, ISTA)[44]), and humidity conditions throughout the campaign.

Water exposure followed two distinct steps. *Initial imbibition*: on the evening preceding D1, seeds in each germinator were soaked in 1 L of their assigned water for approximately 12 h, until the D1 measurement session the following morning. This constituted the first differential water exposure between the two groups; D0 measurements were performed before imbibition and therefore captured pre-treatment baseline emission on dry seeds. *Daily watering*: from D1 to D5, 50 mL of assigned water was applied per germinator after each morning measurement session. TDW was prepared fresh by the Biodynamizer® and applied within the active UPE emission window (t_0, within 30 min of treatment completion), consistent with the protocol applied in the water characterization arm. TW was drawn from the same municipal supply at the time of each TDW preparation.

Measurements were destructive: a germinator assigned to a given session was not reused in subsequent sessions. Each session therefore involved an independent germinator per condition. Day D0 established the pre-treatment UPE baseline on dry seeds (both groups, before imbibition); D0 used 50 dry seeds per tube (see § 4.5). Days D1 to D6 (D = acquisition day) used 24 sprouts per tube and constituted the six measurement sessions used for statistical comparison, for a total of 84 individual measurements (12 germinators × 7 sessions, including D0 baseline). This design follows an established UPE acquisition framework for germinating seeds[10]. Per-sample raw acquisition values (11 replicates per sample) with germinator identifier, day, and condition for the full $N = 84$ dataset are provided in Supplementary Table S2.

4.5 Germination arm: UPE acquisition

At each measurement session (D1–D6), 24 sprouts were extracted from the designated germinator, transferred to a borosilicate glass test tube and placed in the Berthold LB9508 luminometer under the same dark-chamber conditions as the water arm ($k = 11$ consecutive acquisitions per tube; the 380–630

nm spectral response is a characteristic of the instrument's PMT). The arithmetic mean of the 11 acquisitions was taken as the representative RLU s^{-1} cm^{-2} value for that germinator at that session. Background was measured from an empty test tube at each session and subtracted from the gross sample value to obtain the net photon flux density. Session D0 (pre-germination baseline, before imbibition water was assigned) used 50 dry seeds per tube to ensure a signal above the instrument noise floor; both groups produced equivalent emission at D0 (median 222 RLU s^{-1} cm^{-2}, CV < 1%), confirming pre-treatment equivalence before irrigation water was applied. Sessions D1 to D6 (24 sprouts per tube) defined the analysis window.

4.6 Data processing and signal-to-noise ratio

Raw per-sample mean RLU s^{-1} cm^{-2} values were background-corrected by subtracting the empty test-tube measurement obtained in the same acquisition session (intra-session background subtraction). The empty-tube background (24–42 RLU s^{-1} cm^{-2}) represents the cumulative instrumental noise floor: PMT dark current, thermionic emission, detector gain drift, and residual container chemiluminescence[1,2]. Inter-session variability reflects the cumulative contribution of these factors over a six-month measurement period.

Signal-to-noise ratio (SNR) was computed as:

$$SNR = (\mu_{signal} - \mu_{background}) / \sigma_{background}$$

where μ_{signal} is the net mean signal for a given sample, $\mu_{background}$ is the session test-tube background value, and $\sigma_{background}$ is the inter-session standard deviation of background values (σ_{bg} = 5.6 RLU s^{-1} cm^{-2}). Published SNR thresholds of ≥ 3 (adequate detection) and ≥ 5 (strong claim) were applied as quality criteria[2]. Acquisition parameters were confirmed to be identical for test-tube background and sample measurements within each session (parameter isomorphism), which is required for SNR validity. Raw data and processing scripts are openly available in the Zenodo repository[45] (see Data Availability).

4.7 Statistical analysis

Non-parametric tests were selected for both study arms because the group sizes (water arm: n = 11 per group; germination arm: g = 6 germinators per group) are too small to reliably assess normality: the Shapiro-Wilk test has low power for n < 20, and the central limit theorem cannot be invoked. Parametric alternatives (t-test, ANOVA) were therefore not used.

The same non-parametric statistical framework was applied to both study arms. All analyses were performed in Python 3.13.2 (https://www.python.org) using SciPy 1.16.3 (https://scipy.org) for inferential tests, NumPy 2.3.5 (https://numpy.org) for numerical operations, pandas 2.3.3 (https://pandas.pydata.org) for tabular data handling, and matplotlib 3.10.7 (https://matplotlib.org) for figure generation; the bias-corrected and accelerated (BCa) bootstrap confidence intervals were

computed with a custom implementation released with the analysis code. The significance threshold was set at $\alpha = 0.05$.

Mann-Whitney U test. Two-sided Mann-Whitney U tests (scipy.stats.mannwhitneyu, method="asymptotic") compared UPE between treated and control groups within each arm. The asymptotic normal approximation of U with tie-corrected variance was applied throughout both arms[46]. In the water arm, intra-group ties in the control group arise from integer rounding of background-subtracted values and preclude exact permutation testing; the asymptotic mode yields a conservative p-value in this situation. In the germination arm, the same asymptotic mode was applied for consistency and cross-arm comparability, ensuring that p-values from both arms are computed under identical assumptions.

Multiple comparisons (germination arm). Six Mann-Whitney U tests were conducted on the same set of germinators (sessions D1–D6). A Bonferroni correction was applied, setting the session-level significance threshold at $\alpha' = 0.05/6 \approx 0.0083$. All six comparisons remained significant after correction (all $p \leq 5.1 \times 10^{-3} < 0.0083$).

Effect size. Cliff's δ was reported for all pairwise comparisons, computed as $\delta = (n_c - n_d) / (n_1 \times n_2)$, where n_c and n_d are the numbers of concordant and discordant pairs across all inter-group comparisons; $\delta = 1.0$ indicates complete stochastic dominance (every value in one group exceeds every value in the other).

Confidence intervals (water arm). The ratio of medians (TDW/TW) and absolute median difference were reported with 95% bias-corrected and accelerated (BCa) bootstrap confidence intervals (N = 10,000 resamples, fixed random seed)[47].

Preliminary measurements from the first acquisition session (November 2025, Enerlab, Nice, France) have been previously reported[48]. The present study provides the first statistically powered analysis of this phenomenon, incorporating $N = 47$ independent samples across five measurement campaigns and applying formal non-parametric inference and signal-to-noise ratio quantification not performed in the prior report.

4.8 Large language model use

Large language model (LLM) assistance was used during manuscript preparation for text editing and structural organization. All scientific content, data analyses, interpretations, and conclusions are the sole responsibility of the authors.

Declarations

Data Availability

The datasets generated and analyzed during the current study, together with the Python scripts used for all statistical analyses, are openly available in the Zenodo repository at https://doi.org/10.5281/zenodo.21997100[45]. Source data underlying Figures 1–5 are included in the repository.

Author Contributions

C.C. conceived the study and secured funding. O.S. designed the experimental methodology, conducted all luminometric measurements, curated the raw measurement data, and provided laboratory resources. L.S. performed the formal statistical analysis, developed the analysis software, produced all visualizations, and wrote the original manuscript. E.V.d.K. validated the results and critically reviewed and edited the manuscript. All authors read and approved the final version.

Acknowledgements

This work was supported by Dynamized Technologies. The authors thank Matthieu Denoual, Gilles Allegres, and Isabelle Ledoux-Rak for their critical reading of the manuscript. The instrument photographs and the PMT schematic diagram were prepared by the authors.

Funding

Dynamized Technologies provided funding to O.S. (Enerlab) for the conduct of luminometric measurements. L.S. and E.V.d.K. received no funding for this work.

Additional Information

C.C. is the founder of Dynamized Technologies, which funded this study. O.S. is affiliated with Enerlab, an independent laboratory commissioned by Dynamized Technologies to conduct the luminometric measurements. L.S. and E.V.d.K. declare no competing interests.

References

1. Cifra, M. & Pospíšil, P. Ultra-weak photon emission from biological samples: Definition, mechanisms, properties, detection and applications. *J. Photochem. Photobiol B*. **139**, 2–10 (2014).
2. Mould, R. R. et al. Ultra weak photon emission—a brief review. *Front. Physiol.* **15**, 1348915 (2024).
3. Hideg, È., Kobayashi, M. & Inaba, H. Spontaneous ultraweak light emission from respiring spinach leaf mitochondria. *Biochim. Biophys. Acta Bioenerg*. **1098**, 27–31 (1991).
4. Pospíšil, P., Prasad, A. & Rác, M. Role of reactive oxygen species in ultra-weak photon emission in biological systems. *J. Photochem. Photobiol B*. **139**, 11–23 (2014).
5. Devaraj, B. & Biophotons Ultraweak light emission from living systems. *Curr. Opin. Solid State Mater. Sci.* **2**, 188–193 (1997).

6. Saeidfirozeh, H., Shafiekhani, A., Cifra, M. & Masoudi, A. A. Endogenous Chemiluminescence from Germinating Arabidopsis Thaliana Seeds. *Sci. Rep.* **8**, 16231 (2018).
7. Pónya, Z. & Somfalvi-Tóth, K. Modelling biophoton emission kinetics based on the initial intensity value in Helianthus annuus plants exposed to different types of stress. *Sci. Rep.* **12**, 2317 (2022).
8. Yoshinaga, N. et al. Ultraweak photon emission from herbivory-injured maize plants. *Naturwissenschaften* **93**, 38–41 (2006).
9. Tilbury, R. N. The effect of stress factors on the spontaneous photon emission from microorganisms. *Experientia* **48**, 1030–1041 (1992).
10. Gallep, C. D. M. & Robert, D. Time-resolved ultra-weak photon emission as germination performance indicator in single seedlings. *J. Photochem. Photobiol*. **1**, 100001 (2020).
11. De Gallep, M. Ultraweak, spontaneous photon emission in seedlings: Toxicological and chronobiological applications. *Luminescence* **29**, 963–968 (2014).
12. Bertogna, E., Bezerra, J., Conforti, E. & Gallep, C. M. Acute stress in seedlings detected by ultra-weak photon emission. *J. Photochem. Photobiol B*. **118**, 74–76 (2013).
13. Moraes, T. A., Barlow, P. W., Klingelé, E. & Gallep, C. M. Spontaneous ultra-weak light emissions from wheat seedlings are rhythmic and synchronized with the time profile of the local gravimetric tide. *Naturwissenschaften* **99**, 465–472 (2012).
14. Gallep, C. M., Barlow, P. W., Burgos, R. C. R. & Van Wijk, E. P. A. Simultaneous and intercontinental tests show synchronism between the local gravimetric tide and the ultra-weak photon emission in seedlings of different plant species. *Protoplasma* **254**, 315–325 (2017).
15. Pietruszka, M. & Marzec, M. Ultra-weak photon emission from DNA. *Sci. Rep.* **14**, 28915 (2024).
16. Gallep, C. M. & Dos Santos, S. R. Photon-counts during germination of wheat (Triticum aestivum) in wastewater sediment solutions correlated with seedling growth. *Seed Sci. Technol.* **35**, 607–614 (2007).
17. Scholkmann, F., Cifra, M. & Moraes, T. A. De Mello Gallep, C. Using multifractal analysis of ultra-weak photon emission from germinating wheat seedlings to differentiate between two grades of intoxication with potassium dichromate. *J. Phys. Conf. Ser.* **329**, 012020 (2011).
18. Alves Junior, C., De Menezes, F. L. G., Vitoriano, J. D. O. & Da Silva, D. L. Effect of plasma-activated water on soaking, germination, and vigor of Erythrina velutina seeds. *Plasma Med.* **9**, 111–120 (2019).
19. Zhang, S., Rousseau, A. & Dufour, T. Promoting lentil germination and stem growth by plasma activated tap water, demineralized water and liquid fertilizer. *RSC Adv.* **7**, 31244–31251 (2017).
20. Al-Akhras, M. A. H. et al. Impact of magnetized water on seed germination and seedling growth of wheat and barley. *Results Eng.* **22**, 101991 (2024).
21. Zhang, J. et al. Magnetic water treatment: An eco-friendly irrigation alternative to alleviate salt stress of brackish water in seed germination and early seedling growth of cotton (Gossypium hirsutum L). *Plants* **11**, 1397 (2022).

22. Selim, D. A. F. H. et al. Germination, physio-anatomical behavior, and productivity of wheat plants irrigated with magnetically treated seawater. *Front. Plant. Sci.* **13**, 923872 (2022).
23. Liu, Y. et al. Micro-nano bubble water oxygation: Synergistically improving irrigation water use efficiency, crop yield and quality. *J. Clean. Prod.* **222**, 835–843 (2019).
24. Cao, X. et al. Enhancing alfalfa yield via micro-nano bubble oxygenation in subsurface drip irrigation: Rhizosphere mechanisms unveiled by structural equation modeling. *Front. Plant. Sci.* **16**, 1702208 (2025).
25. Oshita, S., Boerzhijin, S., Kameya, H., Yoshimura, M. & Sotome, I. Promotion Effects of Ultrafine Bubbles/Nanobubbles on Seed Germination. *Nanomaterials* **13**, 1677 (2023).
26. Burgos, R. C. R. et al. Ultra-weak photon emission as a dynamic tool for monitoring oxidative stress metabolism. *Sci. Rep.* **7**, 1229 (2017).
27. Chen, H. & Lin, J. M. Ultra-Weak Chemiluminescence from Reaction of Sulfite and Hydrogen Peroxide. in Ultra-Weak Chemiluminescence (eds (eds Lin, J. M., Lu, C. & Chen, H.) 105–126 (Springer Berlin Heidelberg, Berlin, Heidelberg, doi:10.1007/978-3-662-64841-4_6. (2022).
28. Nowak, M. et al. Ultra-Weak Photon Emission from Crown Ethers Exposed to Fenton's Reagent Fe2+-H2O2. *Molecules* **30**, 3282 (2025).
29. Chibowski, E. & Szcześ, A. Magnetic water treatment–a review of the latest approaches. *Chemosphere* **203**, 54–67 (2018).
30. Esmaeilnezhad, E., Choi, H. J., Schaffie, M., Gholizadeh, M. & Ranjbar, M. Characteristics and applications of magnetized water as a green technology. *J. Clean. Prod.* **161**, 908–921 (2017).
31. Alabi, A., Chiesa, M., Garlisi, C. & Palmisano, G. Advances in anti-scale magnetic water treatment. *Environ. Sci. Water Res. Technol.* **1**, 408–425 (2015).
32. Kobe, S., Dražić, G., Cefalas, A. C., Sarantopoulou, E. & Stražišar, J. Nucleation and crystallization of CaCO3 in applied magnetic fields. *Cryst. Eng.* **5**, 243–253 (2002).
33. Cefalas, A. C. et al. Nanocrystallization of CaCO3 at solid/liquid interfaces in magnetic field: A quantum approach. *Appl. Surf. Sci.* **254**, 6715–6724 (2008).
34. Sammer, M. et al. Strong Gradients in Weak Magnetic Fields Induce DOLLOP Formation in Tap Water. *Water* **8**, 79 (2016).
35. Wang, B., Su, H. & Zhang, B. Hydrodynamic cavitation as a promising route for wastewater treatment – a review. *Chem. Eng. J.* **412**, 128685 (2021).
36. Sun, X. et al. A review on hydrodynamic cavitation disinfection: The current state of knowledge. *Sci. Total Environ.* **737**, 139606 (2020).
37. Donepudi, T. *Vortices in Hyperbolic Funnels as Aeration Systems: A Numerical Study* (Delft University of Technology, 2021).
38. Klymenko, R. et al. Enhanced Groundwater Aeration with a Geometrically Constrained Vortex. *Water* **17**, 506 (2025).

39. Nayak, J. K., Ganjare, A. & Ranade, V. V. A Note on Enhancing Aeration via a Vortex-Based Cavitation Device. *ACS Omega*. **10**, 4561–4568 (2025).
40. Kobe, S. et al. Control over nanocrystalization in turbulent flow in the presence of magnetic fields. *Mater. Sci. Eng. C*. **23**, 811–815 (2003).
41. Unterlass, M. Geomimetics and Extreme Biomimetics Inspired by Hydrothermal Systems—What Can We Learn from Nature for. *Mater. Synthesis? Biomimetics*. **2**, 8 (2017).
42. Baumgartner, B., Bojdys, M. J. & Unterlass, M. M. Geomimetics for green polymer synthesis: Highly ordered polyimides via hydrothermal techniques. *Polym. Chem.* **5**, 3771–3776 (2014).
43. Butcher, A. R. & Corfe, I. J. Geo-inspired science, engineering, construction, art and design. *Geol. Today*. **37**, 184–193 (2021).
44. International Seed Testing Association. *ISTA Rules for Seed Testing* (ISTA, Bassersdorf, 2021).
45. Saluden, L. Dataset and Python analysis scripts for 'Ultra-weak photon emission as a dual-axis probe of dynamized water: physicochemical characterisation and germination bioassay'. Zenodo (2026). https://doi.org/10.5281/zenodo.21997100
46. Zar, J. H. *Biostatistical Analysis* (Prentice Hall, 2010).
47. Efron, B. Better Bootstrap Confidence Intervals. *J. Am. Stat. Assoc.* **82**, 171–185 (1987).
48. Salières, O. L. H. Biophotonic evaluation of water treated by biodynamization: Comparison of ultra-low emission levels in the 300–400 nm, 400–500 nm and 500–600 nm bands on different types of water. *South. Fla. J. Dev.* **6**, e6076 (2025).

Figures

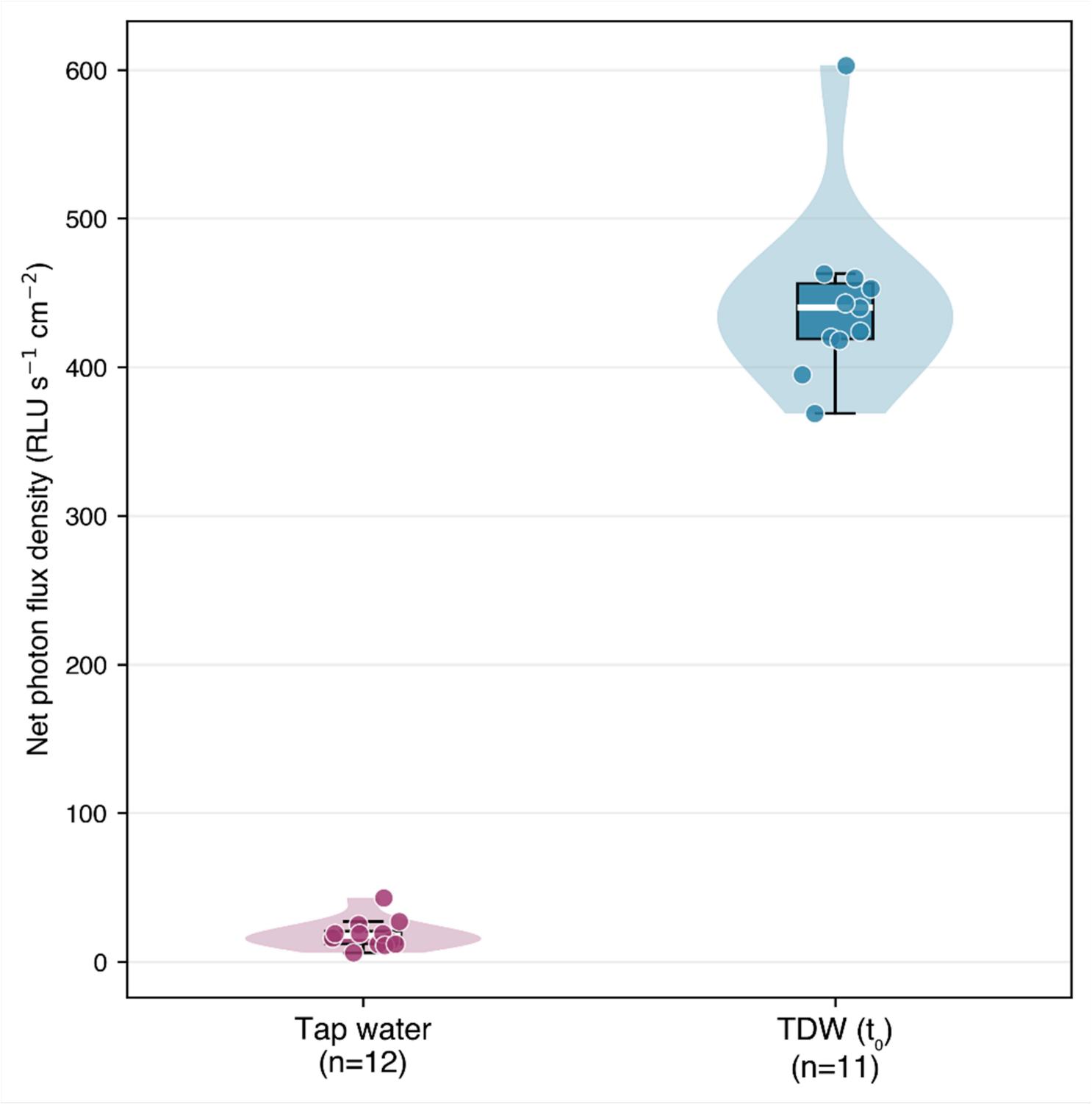


Figure 1

Technologically dynamized water at t_0 emits 27.5-fold more photons than tap water. Net photon flux density (RLU/s/cm²) per sample by group (technologically dynamized water at t_0, TDW; tap water, TW). Violin shapes show where values are most densely concentrated (wider = more observations at that level); boxes: interquartile range (IQR); horizontal bar: median; whiskers: 1.5 × IQR; points: individual measurements. TDW at t_0: *n* = 11 independent preparations across four measurement campaigns

(November 2025 – April 2026); TW: n = 11. Mann-Whitney U = 121, $p = 8.08 \times 10^{-5}$; Cliff δ = 1.0; median ratio 27.5 (BCa 95 % CI [17.0; 36.9]).

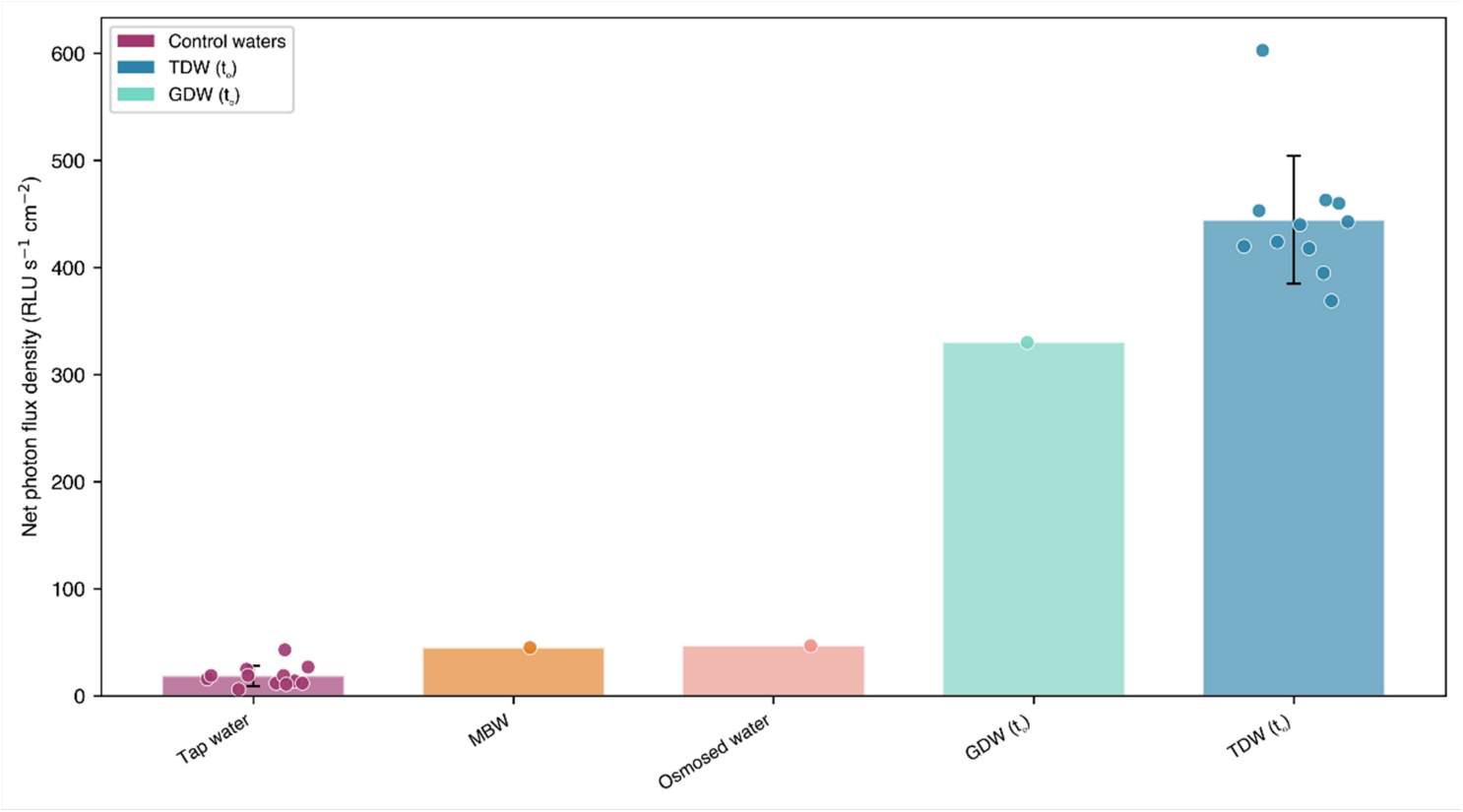


Figure 2

Dynamized water emits above all three control water types (tap, mineral bottled, osmosed). Net photon flux density (RLU s^{-1} cm^{-2}), per sample, sorted within each category. TDW: technologically dynamized water (Biodynamizer® output, measured at t_0); GDW: geologically dynamized water (Vescagne waterfall, measured after transportation); TW: tap water (primary control, same municipal source as TDW pre-processing); MBW: mineral bottled water; OW: osmosed water. TDW (n = 11) and the single GDW measurement emit above all control water types (TW, MBW, OW) across all four measurement campaigns; the single GDW measurement precludes any inferential or ordinal comparison between TDW and GDW.

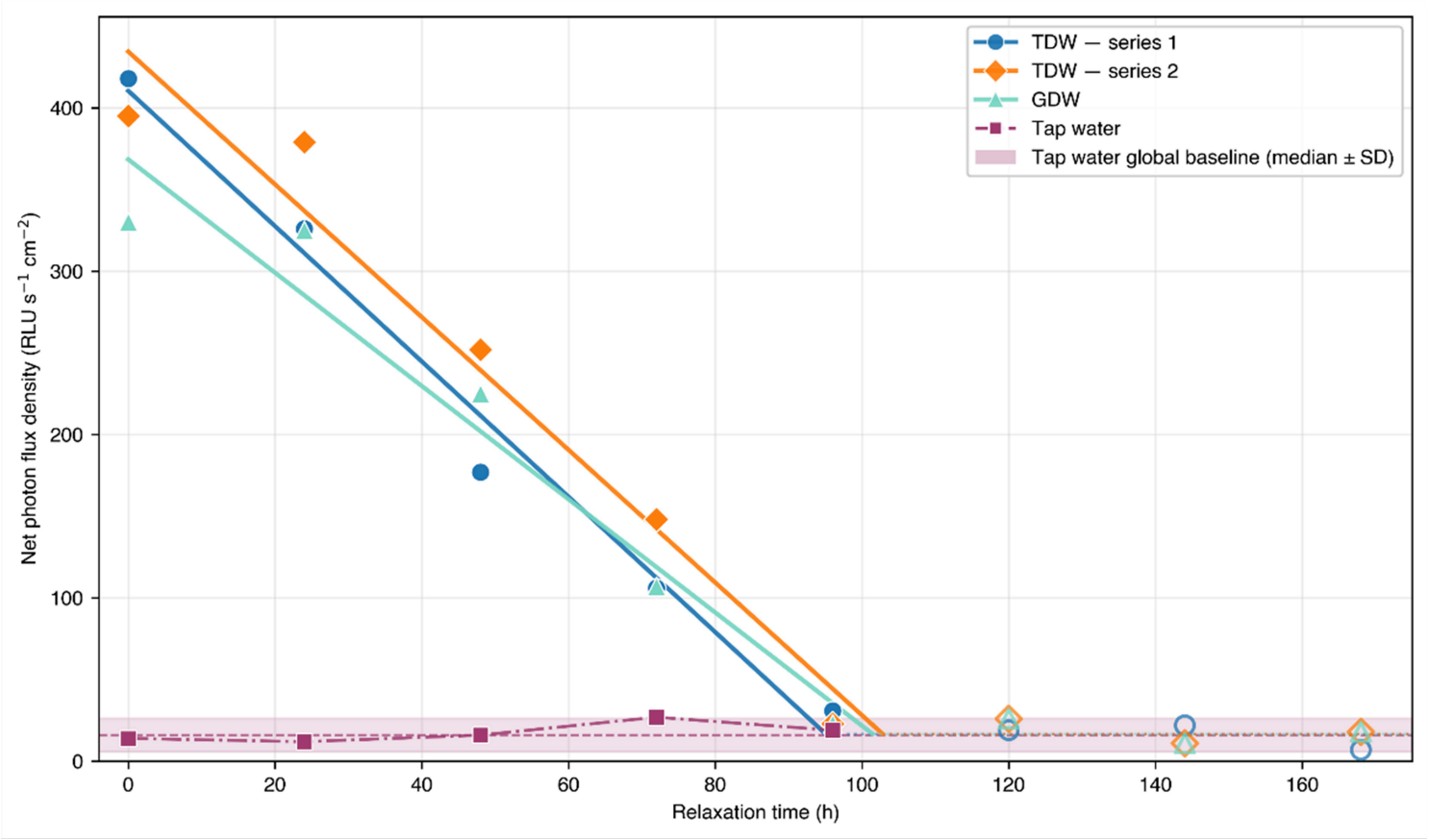


Figure 3

TDW and GDW decay toward the tap water baseline at t=96h. Net photon flux density per sample versus relaxation time (hours), three independent series (two TDW, one GDW). Pink band: TW global baseline (median ± SD, *n*= 11; median = 16 RLU/s/cm², SD = 10 RLU/s/cm²) shown across the full time range as the convergence target. Linear fits restricted to the active decay phase (points reaching the TW global baseline excluded from the fit, shown as open markers). Slopes: TDW series 1, −4.14 RLU/s/cm²/h (R^2 = 0.98, *n*= 5 points); TDW series 2, −4.06 RLU/s/cm²/h (R^2 = 0.96, *n* = 5 points); GDW, −3.47 RLU/s/cm²/h (R^2 = 0.95, *n* = 5 points). Maximum slope gap between TDW and GDW: 0.67 RLU/s/cm²/h (~16 % of the steepest slope). All three series reach the TW global baseline between 95 h (TDW-1) and 103 h (TDW-2), with GDW at ~101 h.

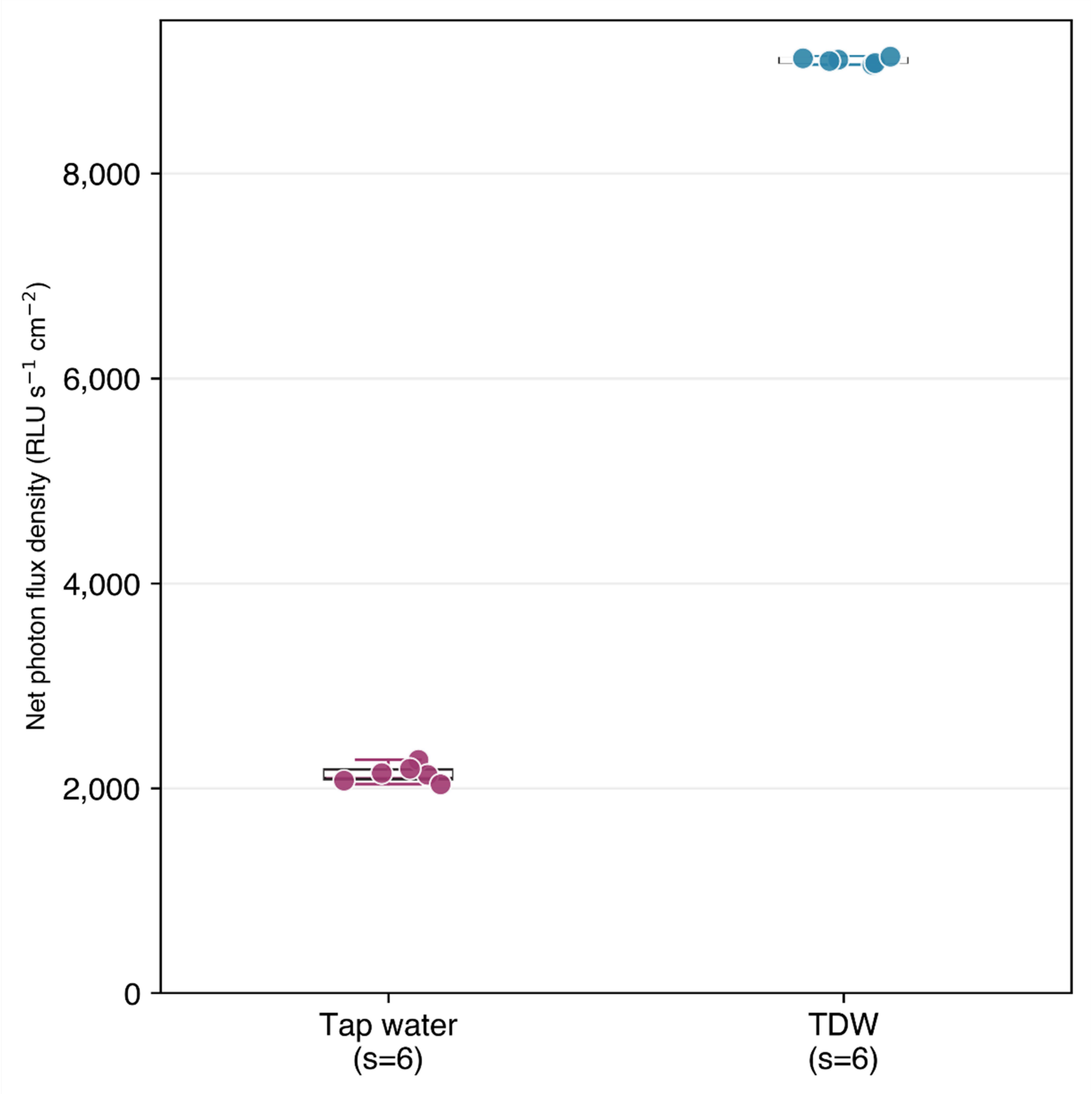


Figure 4

At D6, seedlings watered with technologically dynamized water emit 4.3-fold more photons than tap-water controls. Net photon flux density (group mean, RLU/s/cm²) by acquisition day D1–D6, June 2026 campaign; *g* = 6 germinators per group (TDW-irrigated and TW-irrigated, *Medicago sativa*). D = acquisition day (D1 = first day post-imbibition, D6 = sixth day). The TDW group exhibits an elevated UPE signal from D1 (690 vs 256 RLU/s/cm²) that increases monotonically through D6 (9,107 vs 2,140 RLU/s/cm²). The TW group remains at low, stable levels throughout. Complete stochastic dominance (Cliff δ = 1.0) holds

at every session from D1 to D6; primary endpoint D6: Mann-Whitney U = 36, $p = 5.1 \times 10^{-3}$ (asymptotic, tie-corrected).

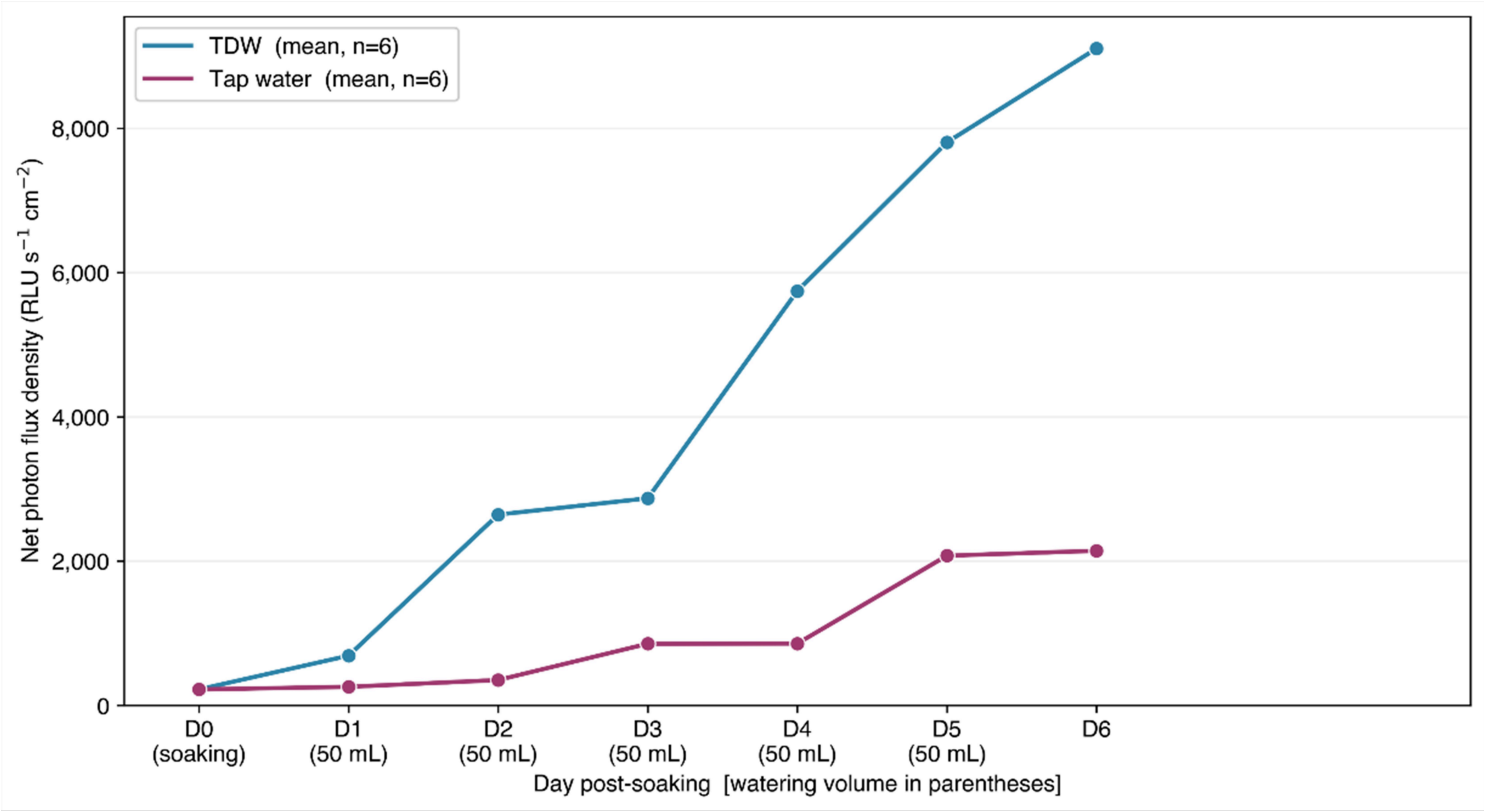


Figure 5

TDW-watered seedlings show monotone UPE growth from D1 to D6 while tap-water controls remain stable. Net photon flux density (group mean, RLU/s/cm²) by acquisition day D1–D6, June 2026 campaign; *g* = 6 germinators per group (TDW: technologically dynamized water; TW: tap water). D = acquisition day. The TDW group shows monotone growth of the UPE signal from D1 to D6 (690 → 9,107 RLU/s/cm²). The TW group remains within the 256–2,140 RLU/s/cm² band with no systematic trend. Inter-group separation increases overall from D1 to D6, with transient narrowing at D3 (ratio 3.3 vs 7.5 at D2; see Table 1).

Supplementary Files

This is a list of supplementary files associated with this preprint. Click to download.

- Saludenetal2026supplementary.docx